Passive Frontal Plane Stabilization in 3D Walking

Sebastian E. Sovero[1], Cenk Oguz Saglam[2] and Katie Byl[2]

***Abstract*— This paper explores the use of a single passive design to stabilize frontal plane dynamics for 3D biped walking across a range of forward velocities and/or step lengths. Particular goals are to determine if design of sagittal plane control can be done independently from design of frontal plane stabilization mechanisms, and to explore how dynamic coupling between the two planned motions affects energetic efficiency of walking. Passive dynamic walkers have long utilized curved feet for low energy frontal plane stabilization in 3D walking, with the current design practice of matching the linearized resonance of the curvature to match a particular, steady-state walking gait to achieve stable coupled limit cycle in the 3D dynamics. However, practical legged walking systems should operate across a range of velocities and step widths. We examine aspects of the nonlinear dynamics that contribute to the energy efficiency and stability of the system through simulations. Specifically, we focus on the frontal plane dynamics and the resulting variability of time-of-return for frontal plane wobbles, as a function of impact velocity. Our decoupled analysis explains some aspects of the 3D motions; however, the actual effects on cost of transport demonstrate interesting phenomena we had not anticipated. Specifically, while a general trend of increasing cost of transport for 3D vs 2D gaits with stride time does hold in our simulations, the 3D gaits sometimes require less energy than their constrained 2D counterparts, which was a surprising and encouraging result. This work provides a promising direction for the development of practical methods to utilize control designed for planar 2D walking models on more sophisticated 3D dynamic models using little or no additional active control.**

I. INTRODUCTION

Legged robotics offer the ability to traverse terrains that are impassable to more traditional wheeled robotics. Existing walking robots do not offer both efficiency and robustness to perturbations [1]. The more traditional ZMP movement robots dynamically constrain the robot for the purpose of guaranteeing dynamic stability [2]. This does provide a conservative criteria for stability [3]. Humans are an inspiration for better energetic efficiency, as they have a mechanical cost of transport of .05 [4]. The advent of passive dynamic robots in the 1980s showed that exploiting the system's natural dynamics could yield stable walking cycles [5]. Active robots have been able to incorporate some of the energy saving mechanism of passive dynamic robots. A recent example is the Cornell ranger robot which demonstrated a cost of transport of .28 in 2010 [6]. In order for legged robots to be practical, we need to lower the cost of transport of existing designs.

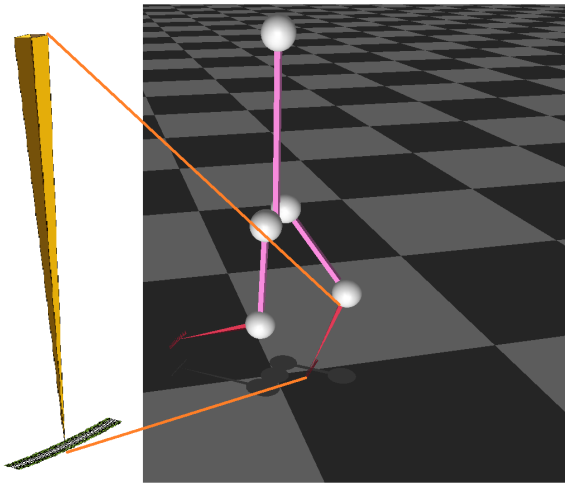

Fig. 1. The Visualization from MuJoCo Simulator is on the right. We placed a magnified view of the curved foot geometry on the left. The center of curvature 80cm above the foot, arc length of 10 °, and a width of 1.8cm

Control of dynamic robots constrained to the sagittal plane has been a focus in our lab [7], [8]. Our sagittal walkers do not exhibit a stable limit cycle in full 3D dynamic simulations. Instead, a yaw-roll instability emerges for these point footwalkers. Experiments based on anthropomorphic data provide evidence that humans require active control to stabilize an unstable mode in the lateral direction [9]. This motivates the need to stabilize humanoid robots in the lateral plane. Biomechanic studies have identified that humans regulate this with ankle torque [10], lateral foothold placement [9], and abduction of the hip laterally [11], [12], [13]. Several dynamic robots have utilized foot shape to stabilize the lateral direction either with yaw-roll coupling[14] or curvature [15]. Yaw-roll coupling uses a phenomenon similar to that seen in skateboards or bicycles, in which small roll deflections induce a yaw, which then corrects the roll [16]. The concept of curved foot walking toys has been around for over a 100 years [17]. The curvature strategy [18] [15] induces a kinematic center of rotation above the center of mass. The center of mass will oscillate as a stable pendulum with dampening provided by rolling friction and impact events.

While there appears to be a potential trade off between stability and cost of transport [19], a robot designer should also

This work is supported in part by NSF Career Award number 1255018.

[1]Sebastian E. Sovero is with the Mechanical Engineering Department at the University of California, Santa Barbara CA 93106 USA sesovero at engineering.ucsb.edu

[2]Katie Byl and Cenk Oguz Saglam are with the Department of Electrical Engineering at the University of Calfornia, Santa Barbara, CA 93106 USA saglam at ece.ucsb.edu, katiebyl at gmail.com

create systems with agility or versatility [20] to navigate the complex terrains of the real world. We make a preliminary exploration of a variety of forward speeds, stride lengths, and stride times. While full 3D dynamics of a robot with multiple degrees of freedom makes analysis difficult, we were able to find trends predicted by the 2D uncoupled dynamics. In this paper we quantify how accurately the 2D dynamics capture the energy efficiency and dynamic nature of the walker. We center our analysis on the link between roll speed to sagittal stepping frequency and energy consumption.

II. Simulator and Models

For the simulations in this paper, we used the MuJoCo Physics Engine developed by Emo Todorov et al. [21]. We use the model parameters of RABBIT for the sagittal plane [22]. The rotational inertias of each link were considered the same in each direction. A more detailed view of the model can be seen in Fig. 1. The lateral separation of the hips, d_{hips} was .2m as shown in Fig. 4. The robot was completely unconstrained in 3D space and did not have any additional actuators than we used in the 2D models.

III. 2D Sagittal Plane System

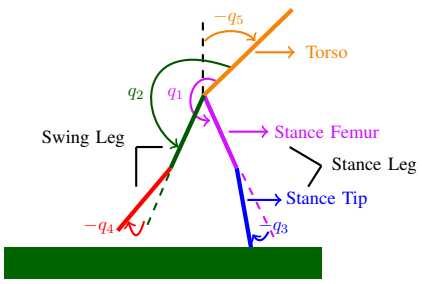

Fig. 2. Diagram of the robot from the sagittal plane

We first consider the dynamics constrained to the sagittal plane (shown in Fig. 2). Because of this constraint there are no frontal plane coupling effects. The continuous dynamics follow the equation

$$D(q)\ddot{q} + C(q,\dot{q})\dot{q} + G(q) = Bu. \tag{1}$$

The 5 links of the walker have 5 joint angles, $q \in [0, 2\pi)^5$; 5 joint velocities, $\dot{q} \in \mathbb{R}^5$; and five joint accelerations $\ddot{q} \in \mathbb{R}^5$. Our robot does not apply any ankle torque making the system underactuated with control input $u \in \mathbb{R}^4$. We utilize a partial feedback linearization control law stated below

$$u = (H_0 D^{-1} B)^{-1}(v + H_0 D^{-1}(C\dot{q} + G)), \tag{2}$$

$$H_0 = \begin{bmatrix} 0 & 1 & 0 & 0 & 1 \\ 0 & 0 & 1 & 0 & 0 \\ 0 & 0 & 0 & 1 & 0 \\ 0 & 0 & 0 & 0 & 1 \end{bmatrix} \tag{3}$$

The feedback linearization allows us to directly set the accelerations of the controlled angles with the variable v. We chose the accelerations by using the sliding surface $\sigma \in \mathbb{R}^4$; convergence exponent α; and convergence coefficient k.

$$v_n = -k_n |\sigma_n|^{2\alpha_n - 1} sign(\sigma_n), \quad n = \{1,2,3,4\}, \tag{4}$$

$$k = \begin{bmatrix} 40.3791 \\ 96.4343 \\ 77.1343 \\ 15.7245 \end{bmatrix} \quad \alpha = \begin{bmatrix} .7003 \\ .6954 \\ .6991 \\ .7001 \end{bmatrix} \quad \tau = \begin{bmatrix} .0920 \\ .0905 \\ .0632 \\ .1918 \end{bmatrix}$$

The sliding surface σ is determined with by the state error h and with time constants τ

$$\sigma_n = \dot{h}_n(t) + h_n(t)/\tau_n, \quad n = \{1,2,3,4\}, \tag{5}$$

The state error h is a function of the current states $q(t)$ and a piecewise reference h_d.

$$h(t) = h_0(t) - h_d \tag{6}$$

$$h_0(t) = \begin{bmatrix} q_5(t) + q_2(t) \\ q_3(t) \\ q_4(t) \\ q_5(t) \end{bmatrix} \tag{7}$$

During the first half of the swing phase, the robot angles satisfy the condition: $q_1(t) + q_5(t) > 180°$. While that condition holds, the reference is:

$$h_d = \begin{bmatrix} 225° & -.968° & -60.0° & TA \end{bmatrix} \tag{8}$$

Otherwise the reference is as follows:

$$h_d = \begin{bmatrix} 180° + FA & -.968° & -24.0° & TA \end{bmatrix} \tag{9}$$

We set the fixed reference parameters k, α, τ, and fixed components for h_d from a sagittal robustness optimization. Refer to [23] for more details. FA is the reference angle corresponding to the absolute angle of the swing leg femur angle at touchdown. Note that the quantity $180° + FA$ corresponds to the absolute angle of the swing femur. The TA is the reference that sets the torso angle while walking

A. Poincare Map of Sagittal System

Note that if the point foot lifts off or slips represented by $p \in \mathbb{R}^2$ and respective foot velocity $\dot{p} \in \mathbb{R}^2$. While our simulation includes all the potential foot dynamics, our standard walking gaits predominately have stationary stance feet. If we consider i to be the step index

$$i = 0, 1, 2, ... \in N, \tag{10}$$

then we can represent the sagittal states as X_i^s to be the state at t_i. Where t_i is the time instant at impact i.

$$X_i^s = \begin{bmatrix} q(t_i) \\ \dot{q}(t_i) \end{bmatrix} \tag{11}$$

We can numerically calculate the Poincare map, Π^s, to the next preimpact time t_i with a particular deterministic controller u_s

$$X_{i+1}^s = \Pi^s(X_i^s, U_s) \tag{12}$$

We have designed a set of sagittal controllers, U_s each with a particular TA and FA reference parameter. If we pick a controller u_s in the set U_s, it has a fixed point, X_d^s. The fixed point has the property:

$$X_d^s = \Pi^s(X_d^s, u_s). \tag{13}$$

This stable fixed point, X_d^s, corresponds to a particular trajectory, which we refer to as the "gait of the robot". Because our sagittal controllers have large basins of attraction, we simply start the walker at a reasonable initial condition and check if it converges within 100 seconds of simulation. We exclude any gaits that do not converge or fall down from our analysis.

The two gait characteristics that we focus on are stride length λ, defined as the distance between the stance and swing foot at impact, and stride time T_s, defined as the time elapsing between impacts. We define G^s as the map that extracts these parameters given an initial condition and controller. We use the fixed point, X_d^s, as the intial condition and a particular controller u_s to determine the limit cycle's gait parameters.

$$(\lambda, T_s) = G^s(X_d^s, u_s) \tag{14}$$

B. Varying Set of Sagittal Controllers

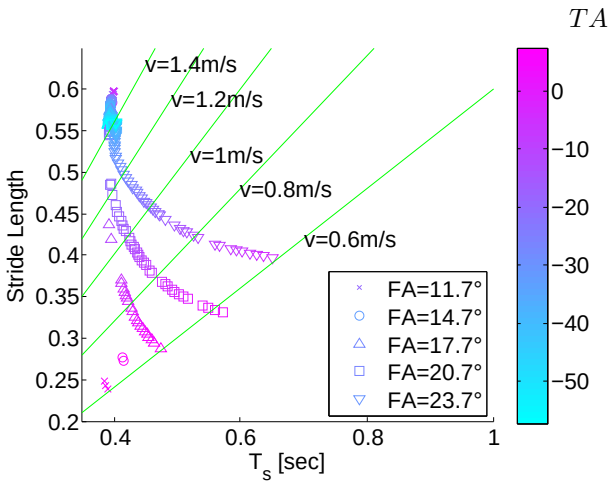

Fig. 3. This figure depicts the gait space spanned by G_s through the variation of two control reference parameters FA and TA. The gait characteristic is at the steady fixed point of the controller on flat ground. The green lines are provided as reference for isocurves of constant forward velocity.

We first adjusted the angle of the torso by varying TA reference angle. In general, forward leaning has been linked to faster forward speeds [24]. As can be seen in Fig. 3, forward torso leaning (negative angles) successfully produces faster walking in our models. This appears to be due to a combination of shorter step times and longer stride lengths. To more fully span the gait space, we also varied the swing femur angle, $q_1(t)$, at touch down through the variable FA. FA has a more direct effect on the step length, because it controls how far the robot extends the swing leg. We tested

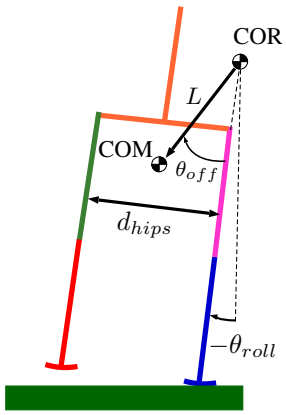

Fig. 4. Each foot has a Center of Rotation (COR) in placed directly above their respective hip. The system behaves very similarly to a stable pendulum with length L. Only there is a pendulum offset θ_{off}

Femur Angle FA from $11.7°$ to $25.7°$ in $3°$ intervals. The Torso Angle TA was from $-57°$ to $7°$ in $.5°$ intervals. We only examined the controllers steady state gait characteristics. Examining transients from various initial conditions and controller switching is a topic of future work. Refer to Fig. 3 for the full details of gaits generated

IV. 2D Frontal Sway Analysis

A. Curved Foot Design

We use the design method from [18] of matching pendulum resonance with the step frequency. Nominally, we started our design with a baseline step period of $T_s = .35s$. The curvature of the foot defines COR (center of rotation). The distance between COR and COM is called the pendulum length, L (refer to Fig. 4). We model the frontal plane simulation with all sagittal joints held statically at $q(t) = 0$. This stable pendulum has a linearized period of

$$T_{pendulum} = (\pi)\sqrt{\frac{L}{g}} \approx .35[s] \ . \tag{15}$$

For our design, we chose $L = 12.21$ centimeters to match our baseline gait. We do not change this parameter for any of the experiments. Our goal is to see the versatility of this fixed curvature design to different types of gaits.

B. Isolated Frontal Plane Dynamics

Note that the $T_{pendulum}$ term is derived using a small angle linearization of the full dynamics, making it an approximation. We therefor consider it more accurate to consider the nonlinear uncoupled frontal plane dynamics. The frontal plane dynamics can be more accurately represented with pendulum length L, total mass $M_t = 32kg$, and rotational inertia of the whole robot, $I_{com} = 6.1kg\ m^2$.

$$(L^2 M_t + I_{com})\ddot{\theta}_{roll} + L\ M_t\ g\ sin(\theta_{roll} + \theta_{off}) = 0 \tag{16}$$

where θ_{offset} is an offset angle defined by the geometry as:

$$\theta_{off} = sin^{-1}\left(\frac{d_{hip}}{2L}\right) \tag{17}$$

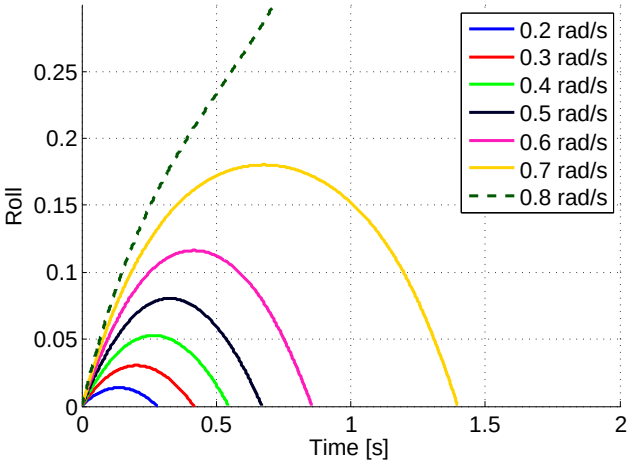

Fig. 5. To determine times of return the model was simulated with various initial roll speeds. The dashed line signifies an initial roll speed in which the robot tips over. Since this trajectory never recovers to $\theta_{roll} = 0$, the time return map is undefined for this velocity.

C. Poincare and Gait Map of Isolated Frontal Plane

The roll dynamics are passive and contain no active control input. We assume slipless contact is maintained by the curved foot. The frontal states are then represented by X_i^f at impact i.

$$X_i^f = \begin{bmatrix} \theta_{roll}(t_i) \\ \dot{\theta}_{roll}(t_i) \end{bmatrix} \tag{18}$$

Where θ_{roll} is the body roll angle, and $\dot{\theta}_{roll}$ is the body roll speed. which we may take Poincare slices at the instant before impact:

$$X_{i+1}^f = \Pi^f(X_i^f) \tag{19}$$

When we simulate the frontal plane in isolation there exists a gait map G^f that for a given initial condition X^f will have T^f time till the next impact.

$$T^f = G^f(X^f) \tag{20}$$

As can be seen by Fig. 6, G^f has an inverse map, G^{-f} defined at T_s. This would correspond to the instance when $T^f = T_s$.

$$X_d^f = G^{-f}(T^s) \tag{21}$$

We assume that X_d^f of the 2D frontal system could be a stable fixed point of the full 3D simulation. While the uncoupled system would not hold on this fixed point due to energy losses (impacts and rolling friction), we assume the coupling from the sagittal plane pumps in sufficient energy.

The assumption of a linearized pendulum might make one expect a flat timing map ($T_{pendulum} = G^f(X^f)$ for all X^f). The actual timing map for the nonlinear oscillator was numerically determined and is shown for the curved foot design in Fig. 6. The timing map prediction was done by simulating the frontal plane system in isolation. A given initial roll speed would correspond to a particular time till next impact. As can be seen in Fig. 6, the 2D uncoupled system closely resembles the full 3D performance. The 3D system has the same general trend that faster roll velocities correspond to longer step times.

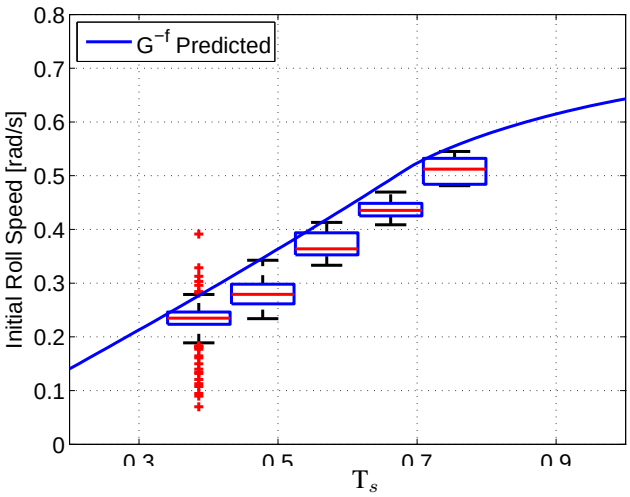

Fig. 6. G^{-f} timing map above is calculated running isolated frontal simulations such as those shown in Fig. 5. The full 3D dynamic simulation is represented with the box and whisker plots. The box is the 25-75% interval, while the bars represent the 9% to 91% interval. Outliers are plotted with red crosses and we suspect they are more prevalent at shorter time steps due to the larger amount of gaits. The frontal plane system behaves overall very similarly to the full 3D dynamical system.

D. 2D Curved Foot Energy Dissipation

Because frontal plane dynamics are passive, we assume the energy must flow from the sagittal to the frontal plane to keep it oscillating. We define $E_{frontal}$ as the extra energy necessary to run the 3D model compared to the 2D model over one step.

We try to approximate the energy lost in the frontal plane with the Hamiltonian, $\mathcal{H}$. The Hamiltonian represents the current energy in the system E_i at step i

$$\mathcal{H}(X_i^f) = Kinetic + Potential = E_i \tag{22}$$

The energy dissipated over one cycle is approximated as:

$$\begin{aligned} E_{frontal} &\approx E_{i+1} - E_i \\ &= \mathcal{H}(\Pi^f(X_d^f)) - \mathcal{H}(X_d^f) \\ &= \mathcal{H}(\Pi^f(G^{-f}(T_s))) - \mathcal{H}(G^{-f}(T_s)) \end{aligned}$$

Our simplified 2D frontal plane analysis shows a prediction in Fig. 7. This prediction trends towards higher energies required at longer step times. This can be explained by greater energy losses from impacts in the frontal plane. As can be see in Fig. 6, longer step times correspond to larger roll velocities during impact events.

While we studied a large number of stable gaits found in 2D and 3D walking, $FA = 20.7$ and $FA = 23.7$ were the only data sets where 3D and 2D gaits were comparable. Parts of these data sets had minimal Stride Time and Stride Length changes from 2D to 3D. As can be seen in Fig. 7 the general trend upheld as predicted by our analysis. Oddly, for shorter stride times, gaits actually became more energy efficient than

their 2D counterparts. The exact mode of whether there is beneficial energy storage in the frontal plane, or shifting of the sagittal gait into more efficient regime is yet to be determined.

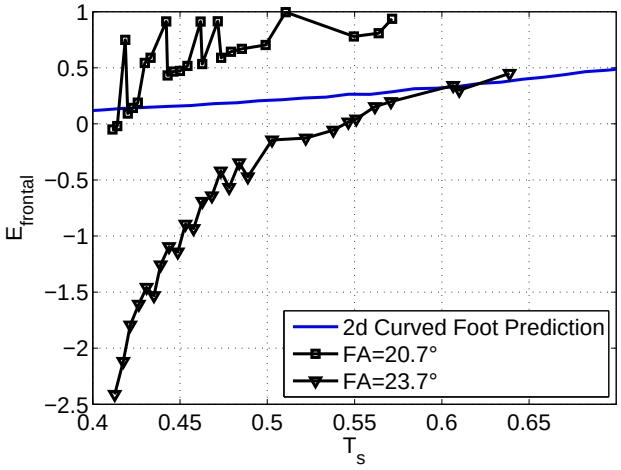

Fig. 7. Difference between in energy of walking 2D sagitally constrained to full 3D dynamics. The units of energy are joules expended during one step cycle. The data sets $FA = 20.7$ and $FA = 23.7$ had minimal changes in the sagittal planes stride length and stride time in 3d. This allowed us to more easily isolate the effect of adding frontal plane dynamics. Note that the sagittal consumption of energy was on the scale of 10 to 35 Joules per step, so this energy expenditure in the frontal plane was a small portion of this.

V. Full 3 Dimensional Dynamics Simulation

A. 3D Shifting of Gait Characteristics

As expected, there was a shift in the gait characteristics of the 3D walking from the 2D model. We suspect that the stride was more susceptible to 3D variations because our controller enforces references dependent on phase variable, not on specific timing. In general due to the slower step times, the walkers walked with slower forward speed. The walking speed variability was due both to changes in Stride Length (Fig. 8) and Stride Time (Fig. 9).

B. Energy Consumption

We define the Mechanical Power flux, P_n at each actuator (n index 1 through 4)

$$P_n(t) = \omega_n \cdot \tau_n \quad n = \{1, 2, 3, 4\} \tag{23}$$

We use two different work metrics for the robot. First we consider conservative work which penalizes both positive work and negative work. Walking gaits had a high amount of variability in performance as can be seen in Fig. 10. We consider this a more accurate representation of the energy required by real actuators such as electric motors.

$$COT_{conservative} = \frac{\int_0^{T_s} \sum_n |P_n(t)| dt}{M_t g \lambda} \tag{24}$$

Finally, the last metric we evaluated was the Net Mechanical energy which assumes that the actuator can recover negative energy. For practical robots, actuator losses make

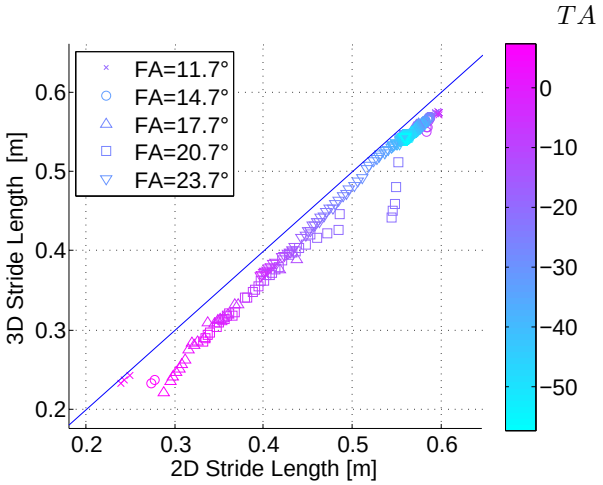

Fig. 8. Step Length change from 2D to 3D. Color bar represents "Torso Angle"

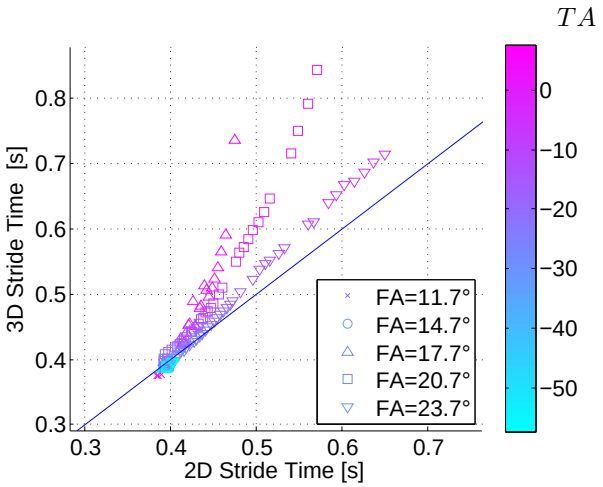

Fig. 9. Stride Time change from 2D to 3D. Color bar represents "Torso Angle"

reaching this level of energy efficiency impossible. Human metabolic cost of transport is 5 to 6 times above the mechanical cost of transport. We instead use this metric to look for increases in energy in going to 3D dynamics.

$$COT_{net} = \frac{\int_0^{T_s} \sum_n P_n(t) dt}{M_t g \lambda} \tag{25}$$

Note as can be seen in Fig. 11 there was a general trend for the COT to go up at higher speeds. Generally, increases in walking speeds cause larger expenditures of energy in humans. The small decrease in energy expenditure in 3D gaits can be explained by short stride times, .35 to .4s, of gaits in the 1.3 m/s range. Remember the trend of energy savings at shorter stride times seen in frontal plane dynamics show in Fig. 7 . The controllers used were not optimized for energy efficiency so a certain amount of variability is expected. We expect 2D energy efficiency variability to also be reflected in the 3D gaits.

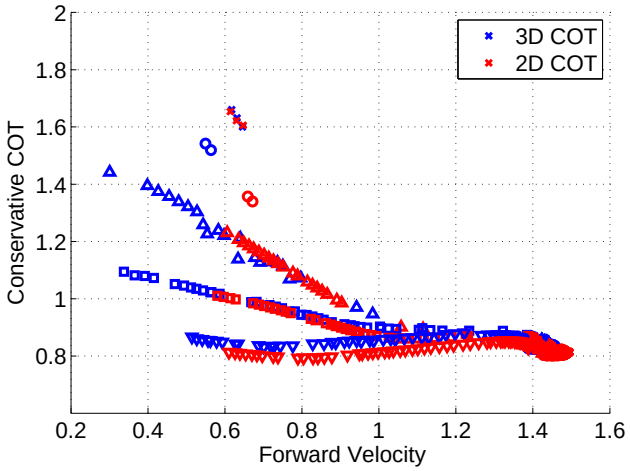

Fig. 10. This COT corresponds to the work in Eq. 24. Interestingly, the conservative COT is not correlated with the trend of the net COT. We suspect the accelerating and accelerations of the legs during the gait slower gaits greatly penalizes the gait. The effect of the frontal plane dynamics appear to be negligible.

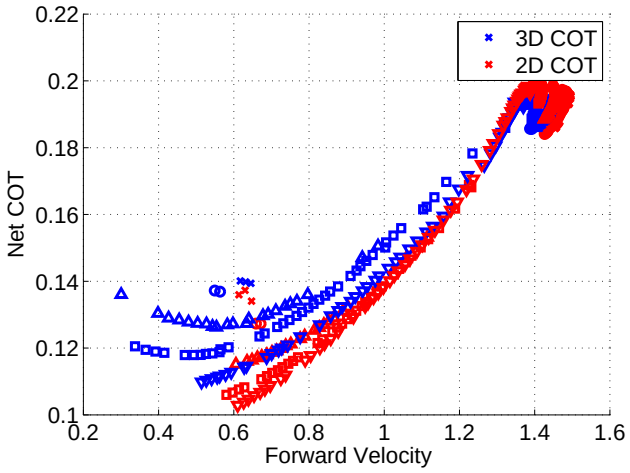

Fig. 11. Cost of Transport corresponding to Eq. 25. Note that in general faster walking speeds correlated with more energy expenditure for the 2D gaits. Remembering that adding the frontal plane dynamics for 3D walking results in energy efficient gaits at shorter stride time (as seen in Fig. 7), we can explain the more efficient 3D walkers at higher speeds (1.2 to 1.5 m/s). The faster walking gaits corresponded gaits corresponded to short stride times of .35 to .4 [s] (Fig. 3)

VI. Conclusion

An uncoupled assumption allowed us to develop the sagittal plane and frontal plane stabilization separately. As expected, there was a shifting in the sagittal gait's stride time characteristics. We mainly saw a shifting of the stride time, as the controller is driven by a phase variable not time reference tracking.

The coupled frontal plane dynamics (Fig. 7) matched closely with our uncoupled prediction. Faster roll speeds were correlated with longer step times. Intuitively, this makes sense - if you push a stable pendulum with more radial speed, it will take longer to return. This dynamic trend correctly predicted higher energy consumption of 3D walkers at shorter stride times. While this general upward trend did hold, there was large variation between data points. We expected this because the 3D dynamics can shift the sagittal gait into a more efficient regime -for example slowing down the walker. As can be seen in Fig. 11, slower forward speeds in the sagittal plane correlated with less energy expenditure. When the 3D walker slows down in the sagittal plane due to coupling, it can shift to a more efficient walking gait. Our methods were good for predicting the general dynamical behavior and general energy trends, but the intricacies of 3D walking introduces a great deal of variability in the data we observed.

VII. Future Work

While the curved foot walker is usually designed for a particular stride frequency, we have show it capable of supporting a variety of 3D dynamical gaits. We are extending these principles to design an active laterally stabilized walker. Our preliminary active lateral stabilization has shown similar energy efficiencies. Additional, we have found techniques for reducing the sagittal gait coupling disturbance. The active lateral stabilization results will be released in a subsequent paper.

For this paper, the sagittal gait map G^s was only tested with steady state limit cycles; it would be interesting to examine its transient solutions. An example being if running the walker in steady state with a certain step length, how quickly can the robot transition to a new step length? This could then be used for online for foothold placement selection, which would be necessary for environments with intermittent footholds. The computability of this map may be challenging due to the high dimensionality of the system ($\mathbb{R}^{22}$), also known at the "curse of dimensionality". We plan to see if our meshing algorithms can be used to reduce the problem's dimension to computationally feasible problem [25].

References

[1] A. D. Kuo, "Choosing your steps carefully," *Robotics & Automation Magazine, IEEE*, vol. 14, no. 2, pp. 18–29, 2007.

[2] M. Vukobratović and B. Borovac, "Zero-moment pointthirty five years of its life," *International Journal of Humanoid Robotics*, vol. 1, no. 01, pp. 157–173, 2004.

[3] A. Goswami, "Postural stability of biped robots and the foot-rotation indicator (fri) point," *The International Journal of Robotics Research*, vol. 18, no. 6, pp. 523–533, 1999.

[4] R. Margaria, "Positive and negative work performances and their efficiencies in human locomotion," *Internationale Zeitschrift für angewandte Physiologie einschließlich Arbeitsphysiologie*, vol. 25, no. 4, pp. 339–351, 1968.

[5] T. McGeer, "Passive dynamic walking," *the international journal of robotics research*, vol. 9, no. 2, pp. 62–82, 1990.

[6] P. A. Bhounsule, J. Cortell, A. Grewal, B. Hendriksen, J. D. Karssen, C. Paul, and A. Ruina, "Low-bandwidth reflex-based control for lower power walking: 65 km on a single battery charge," *The International Journal of Robotics Research*, vol. 33, no. 10, pp. 1305–1321, 2014.

[7] C. O. Saglam and K. Byl, "Stability and gait transition of the five-link biped on stochastically rough terrain using a discrete set of sliding mode controllers," in *Robotics and Automation (ICRA), 2013 IEEE International Conference on*. IEEE, 2013, pp. 5675–5682.

[8] ——, "Switching policies for metastable walking," in *Decision and Control (CDC), 2013 IEEE 52nd Annual Conference on*. IEEE, 2013, pp. 977–983.

[9] C. E. Bauby and A. D. Kuo, "Active control of lateral balance in human walking," *Journal of biomechanics*, vol. 33, no. 11, pp. 1433–1440, 2000.
[10] N. Matsusaka, "Control of the medial-lateral balance in walking," *Acta Orthopaedica*, vol. 57, no. 6, pp. 555–559, 1986.
[11] D. A. Winter, "Human balance and posture control during standing and walking," *Gait & posture*, vol. 3, no. 4, pp. 193–214, 1995.
[12] D. A. Winter, F. Prince, J. Frank, C. Powell, and K. F. Zabjek, "Unified theory regarding a/p and m/l balance in quiet stance," *Journal of neurophysiology*, vol. 75, no. 6, pp. 2334–2343, 1996.
[13] C. D. MacKinnon and D. A. Winter, "Control of whole body balance in the frontal plane during human walking," *Journal of biomechanics*, vol. 26, no. 6, pp. 633–644, 1993.
[14] M. Wisse, "Three additions to passive dynamic walking: actuation, an upper body, and 3d stability," *International Journal of Humanoid Robotics*, vol. 2, no. 04, pp. 459–478, 2005.
[15] S. H. Collins, M. Wisse, and A. Ruina, "A three-dimensional passive-dynamic walking robot with two legs and knees," *The International Journal of Robotics Research*, vol. 20, no. 7, pp. 607–615, 2001.
[16] M. Wisse and A. L. Schwab, "Skateboards, bicycles, and three-dimensional biped walking machines: velocity-dependent stability by means of lean-to-yaw coupling," *The International Journal of Robotics Research*, vol. 24, no. 6, pp. 417–429, 2005.
[17] B. Bechstein, "Improvements in and relating to toys," *UK Patent*, no. 7453, 1912.
[18] R. Tedrake, T. W. Zhang, M.-f. Fong, and H. S. Seung, "Actuating a simple 3d passive dynamic walker," in *Robotics and Automation, 2004. Proceedings. ICRA'04. 2004 IEEE International Conference on*, vol. 5. IEEE, 2004, pp. 4656–4661.
[19] C. O. Saglam and K. Byl, "Quantifying the trade-offs between stability versus energy use for underactuated biped walking," in *Intelligent Robots and Systems (IROS 2014), 2014 IEEE/RSJ International Conference on*. IEEE, 2014, pp. 2550–2557.
[20] D. G. Hobbelen and M. Wisse, *Limit cycle walking*. I-Tech Education and Publishing, Vienna, Austria, 2007.
[21] E. Todorov, T. Erez, and Y. Tassa, "Mujoco: A physics engine for model-based control," in *IEEE Int. Conf. on Intel. Robots and Systems (IROS)*, 2012, pp. 5026–5033.
[22] E. R. Westervelt, J. W. Grizzle, C. Chevallereau, J. H. Choi, and B. Morris, *Feedback control of dynamic bipedal robot locomotion*. CRC press, 2007, vol. 28.
[23] C. O. Saglam and K. Byl, "Quantifying and optimizing stability of bipedal walking gaits," in *IEEE International Conference on Robotics and Automation (ICRA)*, 2015, submitted.
[24] M.-Y. Chen and K. Byl, "Analysis and control techniques for the compass gait with a torso walking on stochastically rough terrain," in *American Control Conference (ACC), 2012*. IEEE, 2012, pp. 3451–3458.
[25] C. O. Saglam and K. Byl, "Robust policies via meshing for metastable rough terrain walking." RSS, 2014.